Electrowinning of copper in two- and three-compartment reactive electrodialysis cells

L. Cifuentes*, M. Grágeda, G. Crisóstomo

Departamento de Ingeniería de Minas, Facultad de Ciencias Físicas y Matemáticas, Universidad de Chile, Tupper 2069, Santiago, Chile

Abstract

Two- and three-compartment copper electrowinning (EW) cells based on reactive electrodialysis (RED) have been studied. The catholyte was cupric sulphate and the anolyte was ferrous sulphate, both dissolved in sulphuric acid. Copper mesh cathodes and graphite bar anodes have been used. The effects of cell current density, temperature, electrolyte recirculation flowrate and nitrogen sparging flowrate on cell performance (cathodic current efficiency, cell voltage and specific energy consumption (SEC)) have been determined. The cell voltage increased with cell current and it decreased with temperature and nitrogen sparging flowrate. The effect of nitrogen sparging flowrate on the cell voltage is stronger than the effect of electrolyte recirculation flowrate, whereas its enhancing effect on mass transfer is stronger than its deleterious effect on electrolyte conductivity. The SEC ranged from 0.94 to 1.39 kW h/kg at cell current densities between 200 and 600 A/m^2. These values are considerably better than those for conventional copper EW (about 2 kW h/kg at 350 A/m^2). The morphology of the electrodeposits has been observed and a comparison between a three-compartment cell and a previously studied squirrel-cage cell (both based on RED) has been drawn.

Keywords: Electrowinning; Electrodialysis; Reaction engineering; Membranes; Mass transfer; Electrochemistry

1. Introduction

The limitations of conventional copper electrowinning (EW) cells and ways to overcome them have been discussed by Cifuentes et al. (2004a, 2005a,b). Various cell designs (including the spouted bed cell and the squirrel-cage cell) have been tested and shown to produce reductions in energy requirements compared with conventional designs. These new cells involve the use of

(a) membranes to separate catholyte from anolyte, hindering cation transport between them;
(b) alternative cathode geometries (particulate or mesh) in order to increase the specific surface area of the cathode;
(c) an alternative anodic reaction ($Fe^{2+} \rightarrow Fe^{3+} + e$) to replace water oxidation to oxygen gas.

However, the need for further work in this area has been pointed out.

This work sets itself two distinct objectives:

(a) To design a copper EW cell which overcomes the shortcomings of conventional EW technology with a simultaneous increase on the energy savings produced by other cell designs, such as the squirrel-cage cell.
(b) To carry out a series of laboratory-scale experiments in order to optimize the energy efficiency of the proposed copper EW cell design.

The spouted bed cell (Scott, 1981, 1988; Stankovic and Stankovic, 1991) and the squirrel-cage cell (Cifuentes et al., 2005a,b) have in common that they are based on moving particulate cathodes. These designs exhibit advantages compared to conventional technology, e.g. increased mass transfer rates and increased specific surface area of the cathode, but they also present disadvantages such as heterogeneous cathodization and physical discontinuity of the particulate cathode.

In the present work simplicity of design was emphasized and, instead of choosing a moving cathode, the movement of the electrolyte relative to a fixed (motionless) cathode was

* Corresponding author. Tel.: +562 678 4510; fax: +562 672 3504.
E-mail address: luicifue@ing.uchile.cl (L. Cifuentes).

enhanced. At the same time, an increased specific cathode surface area (m^2/kg) compared to conventional plate cathodes was warranted by the use of a mesh cathode.

In order to comply with the aforementioned objectives, two side-by-side designs were tested: a two-compartment cell (one for cathode and catholyte and one for anode and anolyte) and a three-compartment cell (one for cathode and catholyte and two for anode and anolyte). The aim of the three-compartment cell is to allow a more homogeneous copper deposition, as it approaches a symmetric distribution of the electric field on both sides of the cathode.

2. Experimental

2.1. Two-compartment cell

The two-compartment RED cell (Fig. 1) was made of acrylic and the compartment dimensions were 65 × 55 × 120 mm^3 each. The cathode and anode compartments were separated by an Ionac MA 3475 anion membrane in order to hinder cation transport between the electrolytes. The membrane is fitted in a 5 cm × 4 cm acrylic window between the compartments; to avoid electrolyte leakage, 2 mm thick rubber seals are placed on both sides of the membrane. Details of membrane pre-treatment have been given elsewhere (Cifuentes et al., 2004a,b).

The composition of the catholyte was 40 g/L Cu (from cupric sulphate) and 190 g/L sulphuric acid. The composition of the anolyte was 56 g/L Fe (from ferrous sulphate) and 190 g/L sulphuric acid. The cathode was made of 99.99% copper mesh with an apparent surface area of 4.95 cm^2 and the anode was made of a graphite bar of the same apparent surface area (4.8 mm diameter and 33 mm height).

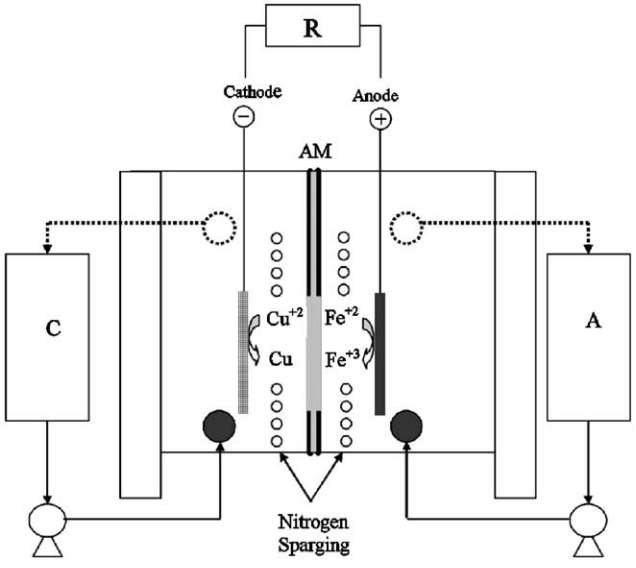

Fig. 1. Two-compartment copper electrowinning cell based on reactive electrodialysis. R = rectifier; AM = anion membrane; A = anolyte container; C = catholyte container.

Table 1
Operating conditions[a] for the two-compartment cell

Experiment	I (A)	i_a, $\lvert i_c \rvert$ (A/m^2)	i_m (A/m^2)	T (°C)
1	0.4	800	200	30
2	0.6	1200	300	30
3	0.8	1600	400	30
4	0.4	800	200	50
5	0.6	1200	300	50
6	0.8	1600	400	50
7	0.4	800	200	60
8	0.6	1200	300	60
9	0.8	1600	400	60

[a]Electrolyte flowrate = 960 mL/ min; 1—sheet mesh cathodes; Catholyte and anolyte volumes = 600 mL; Cell operation time = 4 h; OFN flowrate = 2.5 L/ min.

Copper electrodeposition runs were carried out in order to establish the effect of temperature (30, 50 and 60 °C) and applied cell current (0.4, 0.6 and 0.8 A) on the main cell performance parameters: mass of deposited copper, cell voltage, cathodic current efficiency (CE) and specific energy consumption (SEC). The operation conditions for the two-compartment cell runs are in Table 1. Current densities referenced to the apparent surface area of the membrane (i_m) and to the apparent surface area of anode (i_a) and cathode (i_c) are given.

Electrolyte agitation was achieved by recirculation to ad hoc tanks driven by Watson–Marlow 505S peristaltic pumps. Additional agitation was introduced by oxygen-free nitrogen (OFN) sparging. This was carried out by means of glass tubes immersed in the catholyte fitted with 0.5 mm diameter orifices. Current to drive the cell was provided by a 2 A, 30 V Idisa rectifier. The cathode–anode distance was 20 mm.

In order to characterize the kinetics of the ferrous to ferric ion oxidation at 50 °C, a potentiodynamic sweep was carried out in the two-compartment reactive electrodialysis (RED) cell described above. A Solartron 1286 electrochemical interphase with a 1 mV/s sweep rate was used. The electrolytes (compositions as above) were recirculated at a flowrate of 920 mL/min. The OFN sparging rate was 2.5 L/min. A working electrode made of graphite was used; the counterelectrode was a Pt sheet; the apparent surface area for both electrodes was 4.95 cm^2. The reference electrode was Hg/Hg_2SO_4 with Luggin capillary.

2.2. Three-compartment RED cell

The three-compartment RED reactor was also made of acrylic and it is pictured in Fig. 2. The main purpose of this cell arrangement is to achieve a more evenly distributed copper deposition on both sides of the mesh cathode. In this case the cathode/catholyte compartment is flanked by two anode/anolyte compartments, one on each side. Compartment dimensions were 30 × 56 × 130 mm^3. The already described

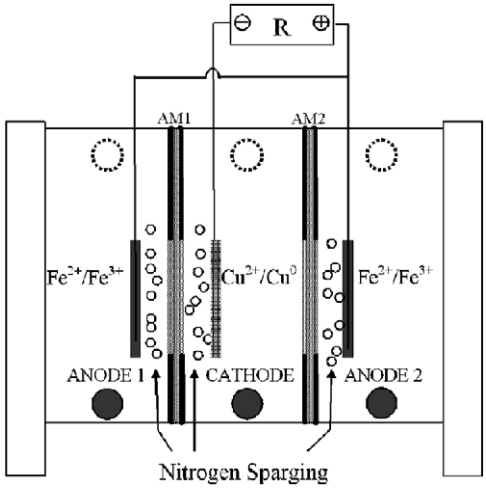

Fig. 2. Three-compartment copper electrowinning cell based on reactive electrodialysis. Electrolyte recirculation is not shown. R = rectifier; AM1, AM2 = anion membranes; A = anolyte container; C = catholyte container.

anion membrane was used to separate each anode/anolyte compartment from the central (cathode/catholyte) compartment. This means that two anion membranes are used in the three-compartment RED cell.

Copper electrodeposition runs were carried out in order to establish the effect of cell current, electrolyte flowrate and nitrogen sparging flowrate on the main cell performance parameters. Three cell current densities (i_m) were applied: 200, 300 and 400 A/m^2. One, two and three-sheet mesh cathodes were used. All experiments were conducted at 50 °C. The cell voltage was monitored throughout the experiments. The operation conditions for the three-compartment cell runs are in Table 2.

The cell was not exactly symmetric. The catholyte compartment required a certain thickness in order to allow for solution sampling, but there was also the need to minimize at least one anode–cathode distance. For these reasons, the anode—membrane distance was 10 mm in both anode compartments, but the distance between the left-hand side membrane (AM 1) and the cathode (see Fig. 2) was 10 mm, whereas the distance between the cathode and the right-hand side membrane (AM 2) was 30 mm.

Cathode and anode dimensions and composition, as well as other design and operation details for the three-compartment cell were the same as described above for the two-compartment cell.

An additional run was carried out at 1000 A/m^2 (referenced to the apparent surface area of the membrane) with the aim of comparing the performance of the three-compartment cell with that of the squirrel-cage cell (Cifuentes et al., 2005a,b)

2.3. Electrodeposit morphology

Macroscopic observations were performed for all the produced electrodeposits and recorded by means of a Nikon Coolpix 4500 camera. There were no major differences in the macroscopic appearance of the deposits produced in various conditions. For this reason, only those deposits produced with the lowest values for cell voltage and SEC are reported. One-, two- and three-sheet mesh cathodes were used.

3. Results and discussion

3.1. Two-compartment cell

3.1.1. Potentiodynamic sweep

To establish the operating cell current range, a potentiodynamic sweep was carried out as described above. The polarization curve is shown in Fig. 3. The limiting current density for the ferrous to ferric reaction on graphite was 1820 A/m^2. This means that the operating cell current density must be below this value in order to avoid the occurrence of the water decomposition reaction to give oxygen gas ($2H_2O \rightarrow O_2 + 4H^+ + 4e$), as this would cause a considerable cell voltage increase, thus increasing the SEC.

3.1.2. Cell performance parameters

Results for average cell voltage, cathodic CE and SEC for various conditions are shown in Table 3.

Results indicate that, at constant temperature, the cell voltage increased with cell current, which is to be expected from a

Table 2
Operating conditions[a] for the three-compartment cell at 50 °C

Experiment	I (A)	i_m (A/m^2)	Electrolyte flowrate (mL/min)	N_2 flowrate (L/min)	No. of Cu sheet layers
1	0.8	200	960	2.5	1
2	0.8	200	1260	—	1
3	0.8	200	1060	2.5	1
4	1.6	400	960	2.5	2
5	1.6	400	1260	—	2
6	1.6	400	1060	2.5	2
7	2.4	600	960	2.5	3
8	2.4	600	1260	—	3
9	2.4	600	1060	2.5	3

[a]Catholyte and anolyte volume = 1990 mL; Cell operation time = 4 h; Cathodic and anodic cell current densities = 1600 A/m^2.

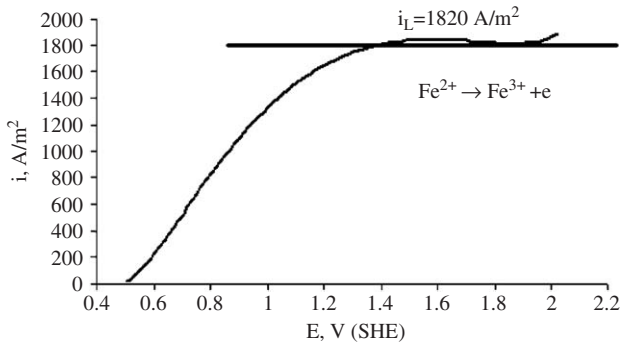

Fig. 3. Potentiodynamic sweep (current density vs. electrode potential) for the $Fe^{2+} \rightarrow Fe^{3+} + e$ anodic reaction. $T = 50\,^{\circ}C$, [Fe(II)] = 56 g/L, graphite anode.

reaction taking place under mixed control. The kinetics, in this case, are given by expressions derived from Fick's law and from high-field approximations to the Butler–Volmer equation (Cifuentes et al., 2004a, 2005a,b).

For the cathodic reaction, the equation is

$$|i_c| = \frac{i^b_{0,c}|i_{L,c}|}{i^b_{0,c} + |i_{L,c}| \exp((\alpha_c F/GT)\eta_c)} \quad (1)$$

and for the anodic reaction:

$$i_a = \frac{i^b_{0,a} i_{L,a}}{i^b_{0,a} + i_{L,a} \exp((-\alpha_a F/GT)\eta_a)}. \quad (2)$$

For the two-compartment cell, the cell voltage is given by

$$V_{\text{cell},2c} = \Delta E_e + \eta_a + |\eta_c| + I(R_a + R_c + R_m) \quad (3)$$

and the energy required to drive the cell is

$$W = V_{\text{cell}} It. \quad (4)$$

At constant current, the higher the temperature, the lower the cell voltage. This is because higher temperatures cause higher ion diffusivities, higher electrolyte conductivities, lower electrical resistances for anolyte and catholyte (R_a, R_c) and enhanced mass transport, which increases the limiting current densities ($i_{L,a}$, $i_{L,c}$), resulting in a decrease of the overpotentials (η_a, $|\eta_c|$). Eq. (3) shows that both the decrease in electrolyte resistance and overpotential cause a reduction in cell voltage.

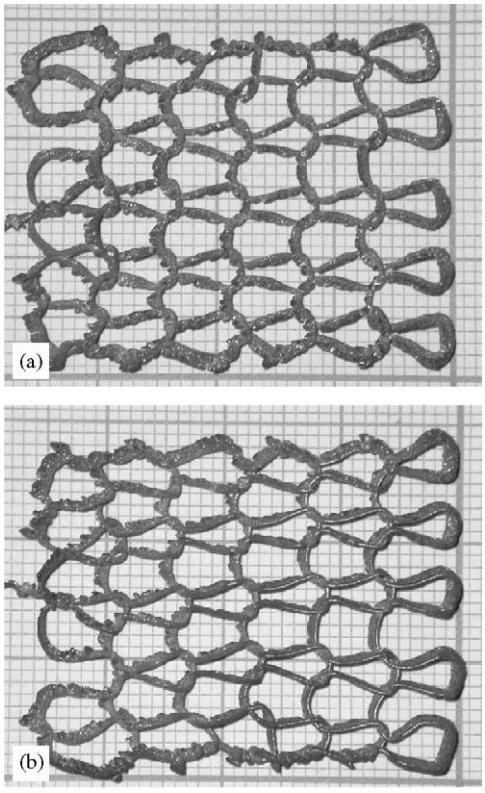

Fig. 4. Electrodeposits obtained on single-sheet mesh cathodes. $i = 800\,A/m^2$, $T = 50\,^{\circ}C$. (a) front face and (b) back face.

Table 3 shows that in all experiments the cathodic CE was higher than 95% and the SEC was between 26% and 67% lower than the values obtained in conventional Cu EW (about 2 kW h/kg of produced Cu). These energy savings (see Eq. (4)) are significant, as shown by Experiment 9, where at $400\,A/m^2$ and 60 °C, the SEC was about 50% of the conventional value.

3.1.3. Electrodeposit morphology

The electrodeposits obtained at 30 °C (Table 1) do not cover all the cathode surface and exhibit a marked dendritic

Table 3
Results for two-compartment cell[a]

Experiment	Cell voltage (V)	Deposited Cu mass (g)	Cathodic current efficiency (%)	Specific energy consumption (kW h/kg Cu)
1	1.10	1.861	98.2	0.95
2	1.42	2.770	97.4	1.23
3	2.42	3.760	99.2	2.06
4	0.78	1.871	98.7	0.66
5	1.06	2.811	98.8	0.91
6	1.38	3.670	96.8	1.47
7	0.74	1.808	95.3	0.66
8	1.05	2.783	97.8	0.91
9	1.24	3.772	99.5	1.05

[a]Experimental conditions are in Table 1.

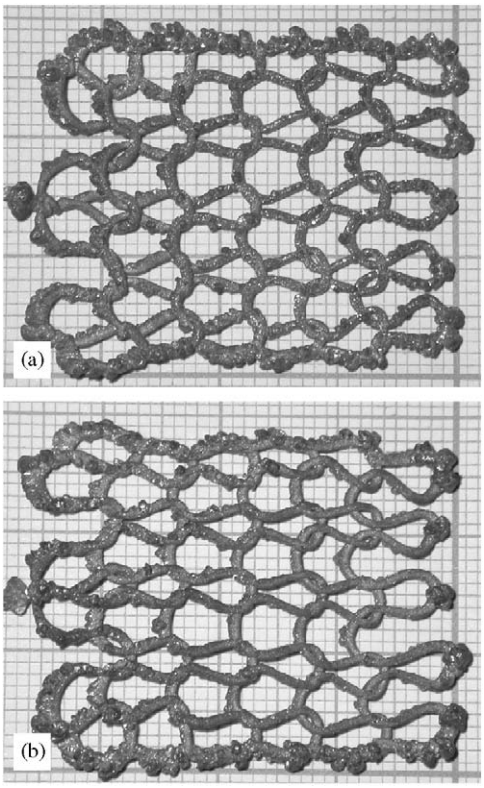

Fig. 5. Electrodeposits obtained on single-sheet mesh cathodes. i=1600 A/m^2, T = 50 °C. (a) front face and (b) back face.

morphology. Those obtained at 50 and 60 °C present similar features: surface coverage is 100% on both cathode faces and the membrane-side face exhibits a greater amount of deposit in comparison with the back face.

Deposits obtained at a current density of 800 A/m^2 (referenced to cathode surface area) and temperatures of 50 °C are shown in Fig. 4 (a) (front face) and Fig. 4(b) (back face).

The electrode side which faces the membrane (front face) exhibits dendritic growth. The dendrites grow in an upward direction, which coincides with the direction in which the nitrogen bubbles flow. The back face presents deposit-free zones.

In Fig. 5 the cell current density (1600 A/m^2) is twice as large as in Fig. 4. At this cell c.d., there is full coverage on both sides of the electrode, but the deposit thickness on the front face is greater than in the back face. It is also to be noted that at both current densities there is more deposit at the cathode edges than at the centre. This edge effect has been previously studied by Cifuentes and Mella (2006). The space distribution of current density and potential in an electrochemical reactor influence local reaction rates and surface phenomena such as the growth of dendrites and nodules in electrocrystallization. These phenomena are significant in determining the physical quality of the cathode.

The morphology of the deposits shown in the present work are indicative of a tertiary distribution of cell current and potential, where electric field, charge transfer and mass transfer effects are significant. The reactant concentration gradients and limiting current densities are important, so that the current density distribution depends on both the distribution of the electric field and the hydrodynamics of the electrolyte.

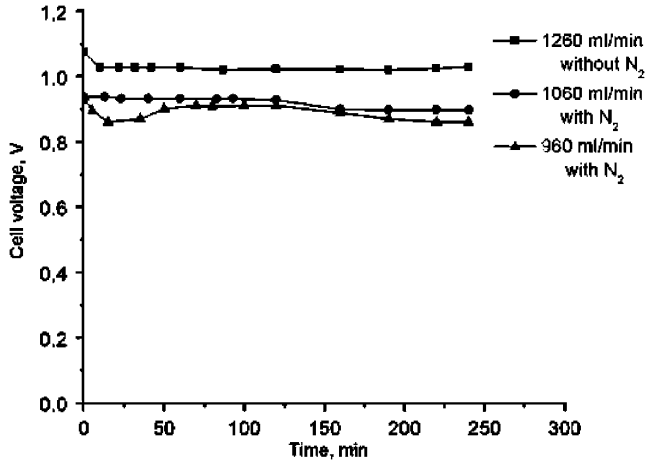

Fig. 6. Cell voltage vs. time as a function of electrolyte recirculation flowrate and OFN sparging flowrate. One-sheet cathodes, I = 0.8 A.

In all cases, a thicker deposit is observed at the cathode edges than at its centre. This edge effect increases with the applied current as shown by Figs. 4 and 5.

3.2. Three-compartment cell

The performance of the three-compartment cell was studied. The effect of electrolyte flowrate and nitrogen sparging flowrate on the main cell performance parameters was established.

For the three-compartment cell, the cell voltage is given by

$$V_{\text{cell},3c} = \Delta E_e + \eta_a + |\eta_c| + I(R'_{a1} + R'_c + R'_{a2} + 2R_m) \quad (5)$$

as there are two anode/anolyte compartments and two anion membranes in the design. The electrical resistance of catholyte and anolyte is given by

$$R = \frac{1}{\kappa}\frac{d}{A}, \quad (6)$$

where d is the distance travelled by ions in the corresponding electrolytes (e.g., between membrane and electrode).

The increased energy consumption for the three-compartment cell, compared to the two-compartment one, may be justified by a much more homogeneous deposition on the mesh cathode caused by the more symmetric distribution of the electric field.

3.2.1. Cell voltage against time

Figs. 6–8 show the variation of the cell voltage with time for the three-compartment cell.

The highest cell voltages were produced without OFN sparging, despite the fact that in all three cases the electrolyte recirculation flowrate was highest (1260 mL/min). This clearly indicates that the effect of OFN sparging on cell voltage is more significant than the effect of the electrolyte recirculation flowrate. This is due to cell design, as the manifold which feeds nitrogen to the cell is placed right underneath the cathode and therefore it promotes electrolyte turbulence at the cathode

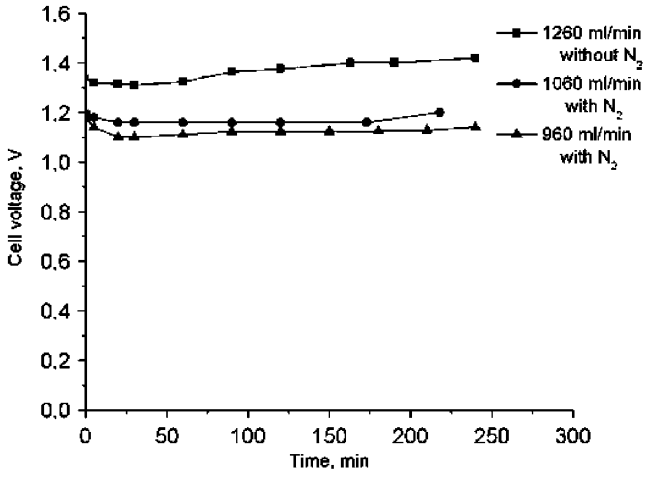

Fig. 7. Cell voltage vs. time as a function of electrolyte recirculation flowrate and OFN sparging flowrate. Two-sheet cathodes, $I = 1.6$ A.

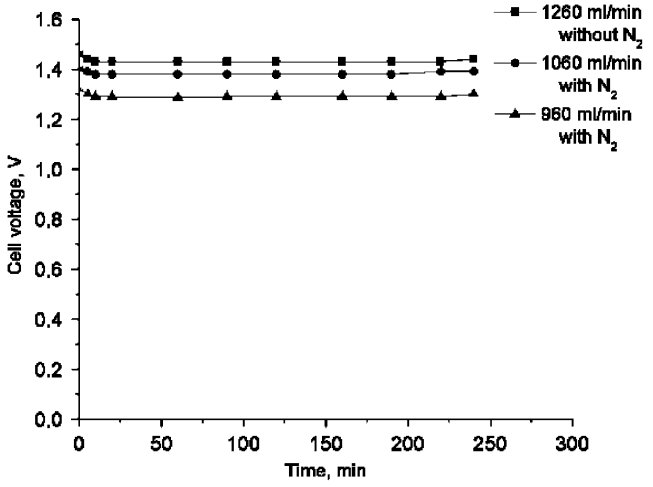

Fig. 8. Cell voltage vs. time as a function of electrolyte recirculation flowrate and OFN sparging flowrate. Three-sheet cathodes, $I = 2.4$ A.

face, thus enhancing mass transfer, reducing the diffusion layer thickness, increasing the limiting current density for copper deposition and causing a decrease in the cell voltage.

The same effect is present in the anode/anolyte compartments, where nitrogen is fed in the same fashion, causing a reduction in the overpotential of the anodic reaction.

As a result of these effects, in the absence of sparging, the cell voltage increases.

The observed cell voltage reduction under OFN sparging takes place despite the fact that the moving gaseous phase (OFN) results in electrolyte discontinuities which would be expected to decrease the electrical conductivity of the solution, thus increasing its resistance and cell voltage. The conclusion is that the enhancing effect of nitrogen sparging on mass transfer is, in the studied conditions, stronger than its potentially deleterious effect on electrolyte conductivity.

3.2.2. Current efficiency and specific energy consumption

Table 4 shows similar trends as those exhibited by the two-compartment cell. The cell voltage and SEC are, as expected, higher for the three-compartment design. Cathodic efficiency ranged from 98% to 99%, while the SEC ranged from 0.94 to 1.39 kW h/kg at cell current densities between 200 and 600 A/m^2. The energy consumption values are considerably lower than those for conventional copper EW (about 2 kWh/kg at 350 A/m^2).

3.2.3. Comparison with the squirrel-cage cell

An additional experiment was carried out at a cell current density (i_m) of 1000 A/m^2 in order to allow a comparison of the performance of the three-compartment cell with results obtained with the squirrel-cage cell (Cifuentes et al., 2005a,b). The latter cell is very similar to the two-compartment cell, but it exhibits a particulate cathode which moves inside a rotating squirrel-cage-type enclosure. Results are presented in Table 5. These results show that, at 1000 A/m^2, both the cell voltage and the SEC are lower (i.e., better) for the three-compartment cell than for the squirrel-cage cell. Given the fact that the cathodic CE is also better for the three-compartment cell, there is no doubt that the latter cell represents a superior design. Its main advantages are simplicity of design and a static mesh cathode in a solution agitated by nitrogen sparging, which provides better results than a moving particulate cathode. The advantages of the three-compartment cell design are (a) better physical continuity of the mesh cathode compared to the particulate cathode and (b) enhanced mass transfer caused by localized nitrogen sparging on the turbulence-promoting mesh cathode compared to the combined movement of the particulate cathode and electrolyte in the squirrel-cage cell.

3.2.4. Morphology of electrodeposits

To the naked eye there is little difference between the physical aspect of the electrodeposits, therefore, it was decided to analyse those produced with better (lower) cell voltage and SEC values. These were obtained on one-, two- and three-sheet mesh cathodes. The electrodeposition conditions were: 1600 A/m^2 cell current density, 960 mL/min electrolyte recirculation flowrate and 2.5 L/min OFN flowrate. In Figs. 9–11, *A* is the cathode's front face (facing the membrane) and *B* is its back face.

Fig. 9 shows that the electrodeposit obtained in the three-compartment cell is homogeneous and similar on both faces of the cathode. An edge effect (preferential deposit growth at the cathode edges) is apparent.

The deposit in Fig. 10 shows very similar morphology to Fig. 9: it is homogeneous, similar on both faces and it also exhibits an edge-effect.

Fig. 11 shows similar features to Fig. 10, only that the edge-effect is strongly accentuated and the mesh geometry is altered due to partial closing of its spacing.

The same considerations made above regarding the morphology of the electrodeposits obtained in the two-compartment cell also apply in this case. The only difference is that the

Table 4
Results for three-compartment cell[a]

Experiment	Cell voltage (V)	Deposited Cu mass (g)	Cathodic current efficiency (%)	Specific energy consumption (kW h/kg Cu)
1	1.11	3.769	99.1	0.94
2	1.21	3.742	98.7	1.04
3	1.29	3.792	99.5	1.09
4	1.31	7.575	99.7	1.11
5	1.54	7.558	99.5	1.31
6	1.36	6.845	99.2	1.15
7	1.48	11.019	98.9	1.27
8	1.62	10.866	98.4	1.39
9	1.57	10.921	98.4	1.35

[a]Experimental conditions are in Table 2.

Table 5
Comparison between the three-compartment cell and the squirrel-cage cell[a]

Cell	Cathode	Cell voltage (V)	Current efficiency (%)	SEC[b] (kW h/kg Cu)
Three-comp.	Single Cu mesh sheet (static)	1.80	94	1.60
Squirrel cage	Cu granules (moving)	1.91	90	1.67

[a]Data for the squirrel-cage cell from Cifuentes et al. (2005a,b).
[b]SEC = specific energy consumption.

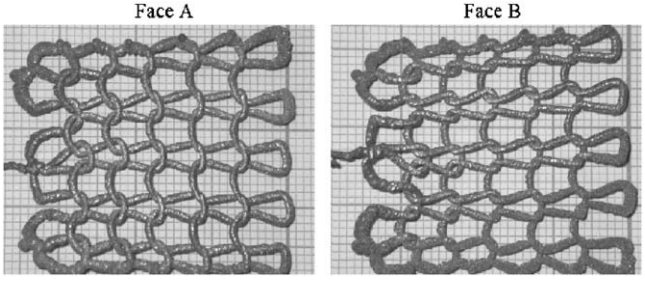

Fig. 9. Electrodeposit obtained on a single-sheet cathode in the three-compartment cell. $I = 0.8$ A. Other conditions in Table 2. Face A is closest to the membrane.

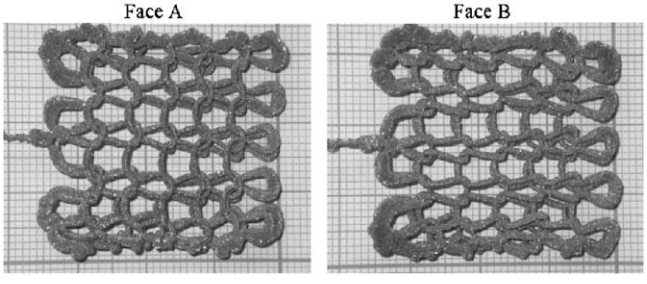

Fig. 10. Electrodeposit obtained on a two-sheet cathode in the three-compartment cell. $I = 1.6$ A. Other conditions in Table 2. Face A is closest to the membrane.

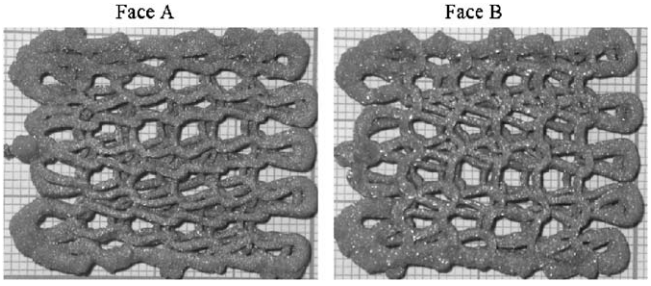

Fig. 11. Electrodeposit obtained on a three-sheet cathode in the three-compartment cell. $I = 2.4$ A. Other conditions in Table 2. Face A is closest to the membrane.

deposition is much more homogeneous on both sides of the cathode due to the more symmetric electric field.

From Figs. 9–11 the importance of the cell current on the production of the electrodeposit becomes apparent, as much bulkier deposits are produced at the highest cell current.

3.2.5. Fe(III) production in the anolyte

In the present work, the Fe(III) production rate for a Fe(II) concentration of 56 g/L and a cell current density of 600 A/m^2 was 2.5×10^{-3} kg/h, which is similar to previously reported results for EDR cells (Cifuentes et al., 2005b). The latter publication describes the methodology for the quantitative analysis of Fe species.

The resulting ferric solution can be used as a starting point for the hydrothermal precipitation of ferric sulphate and ferric oxide, both of which have considerable commercial value; on the other hand, ferric solutions are strongly oxidizing and can be used as leaching agents in hydrometallurgical processing. Both possibilities enhance the economic viability of the proposed process.

3.2.6. Comments on scale-up

This work did not include experimental scale up of the studied cells. As discussed for the squirrel-cage cell (Cifuentes et al., 2005a), among the components of the cell voltage for the

Table 6
Cell voltage quantification (in V) for deposition at 1000 A/m^2 in the three-compartment cell for three-cell configurations[a]

Config.	ΔE_e	η_a	$\lvert\eta_c\rvert$	IR_a	IR_c	IR_m	V_{cell}
1	0.40	0.15	0.05	0.25	0.55	0.40	1.80
2	0.40	0.15	0.05	0.25	0.27	0.40	1.52
3	0.40	0.15	0.05	0.50	1.08	0.40	2.58

For Configuration 1, the overall cell voltage was measured. The values for the components of V_{cell} were estimated from data by Cifuentes et al. (2004a,b, 2005). Anode and membrane numbers refer to Fig. 2.

[a]

Configurations (distances in mm)	1	2	3
Distance anode—membrane 1	10	10	10
Distance membrane 1—cathode	10	10	40
Distance cathode— membrane 2	30	10	40
Distance membrane 2—anode 2	10	10	30
Total distance anode 1—anode 2	60	40	120

three-compartment cell (Eq. (5)), at constant electrolyte composition and temperature, the overpotentials of the anodic and cathodic reactions, as well as the ohmic drops across membranes, depend on cell current density and local mass transport phenomena and are independent of the size of the reactor. The equilibrium potential difference remains constant with cell size, thus only the potential drops in anolyte and catholyte are direct functions of cell geometry, i.e., functions of the distance between anode and cathode, factors which should be considered in an eventual scale up.

In the present case (see Fig. 2), the relevant distances are anode 1—membrane 1 (AM1), membrane 1—cathode, cathode—membrane 2 (AM2) and membrane 2—anode 2, where "1" corresponds to the left-hand side of Fig. 2 and "2" corresponds to the right-hand side of the same figure.

Table 6 shows the effect of various electrode—membrane distances on the cell voltage. For configuration 1, which corresponds to the three-compartment cell used in this work, the measured cell voltage was 1.80 V.

For configuration 2, the distance between cathode and membrane 2 decreases from 30 to 10 mm compared to configuration 1, and this is reflected in the calculated cell voltage, which drops from 1.80 to 1.52 V (a 16% decrease).

For configuration 3, the distance between membrane 1 and cathode increases from 10 to 40 mm, the distance between cathode and membrane 2 increases from 30 to 40 mm and the distance between membrane 2 and anode 2 increases from 10 to 30 mm compared to configuration 1, with a resulting 2.58 V for the calculated cell voltage (a 43% increase). This shows the importance of cell dimensions on the energy requirements to drive the cell (Eq. (4)).

4. Conclusions

(1) At constant temperature, the cell voltage of the two-compartment cell increased with cell current, which is to be expected from a reaction taking place under mixed control.
(2) At constant current, the cell voltage of the two-compartment cell decreased with increasing electrolyte temperature. This is because higher temperatures cause higher ion diffusivities, higher electrolyte conductivities, lower electrical resistances and lower limiting current densities, resulting in a decrease of the overpotentials and of the cell voltage.
(3) The effect of increasing OFN sparging flowrate on the cell voltage is to reduce it. This is because localized OFN sparging promotes electrolyte turbulence at the cathode face, thus enhancing mass transfer, reducing the diffusion layer thickness, increasing the limiting current density for both copper deposition and ferrous ion oxidation, thereby causing a decrease in the cell voltage.
(4) The enhancing effect of nitrogen sparging on mass transfer is, in the studied conditions, stronger than its deleterious effect on electrolyte conductivity.
(5) In the three-compartment cell, cathodic current efficiency (CE) ranged from 98% to 99%, while the specific energy consumption (SEC) ranged from 0.94 to 1.39 kW h/kg at cell current densities between 200 and 600 A/m^2. The energy consumption values are considerably lower than those for conventional copper electrowinning (about 2 kW h/kg at 350 A/m^2).
(6) A comparison between the results of the three-compartment cell with those obtained with a squirrel-cage cell (with a moving particulate cathode), indicates that both the cell voltage and the SEC are lower (i.e., better) for the three-compartment cell at $i_m = 1000\ \mathrm{A/m^2}$. The cathodic CE is also better for the three-compartment cell, which confirms that it represents a superior design.
(7) Calculations point to the importance of cell dimensions on cell voltage and energy requirements. Different electrode-membrane distances result in cell voltages from 1.52 to 2.54 V (a 67% difference) for the three-compartment RED cell.

5. Further work

Work continues on the effect of impurities and additives on the physical and chemical properties of the electrodeposits in the three-compartment reactive electrodialysis cell. Mathematical modelling of the studied cells is also in progress.

Notation

D	diffusivity, $m^2\,s^{-1}$
E_e	equilibrium potential, V
F	Faraday's constant, $C\,eq^{-1}$
G	gas constant, $J\,mol^{-1}\,K^{-1}$
i_a	current density for an anodic reaction, $A\,m^{-2}$
i_c	current density for a cathodic reaction, $A\,m^{-2}$
$i_L, i_{L,a}, i_{L,c}$	limiting current density, anodic and cathodic, $A\,m^{-2}$
$i_0, i_{0,a}, i_{0,c}$	exchange current density, anodic and cathodic, $A\,m^{-2}$
I	cell current, A
$(IR)_a$	potential drop in anolyte, V
$(IR)_c$	potential drop in catholyte, V
$(IR)_m$	potential drop in membrane, V
R, R'_{a1}, R'_{a2}	electrical resistance, anolyte 1 and anolyte 2, Ω
t	time of cell operation, s
T	temperature, K
V_{cell}	cell voltage, V
W	cell driving energy, J

Greek letters

$\alpha, \alpha_a, \alpha_c$	charge transfer coefficient, anodic and cathodic
ΔE_e	difference between E_e values of anodic and cathodic reactions, V
η, η_a, η_c	overpotential, anodic and cathodic, V

Acknowledgements

This work was funded by the National Committee for Science and Technology (CONICYT, CHILE) via FONDECYT Project no. 101 0138. Financial support from Placer Dome to the Chair of Environmental Studies in Mining and continued support from the Department of Mining Engineering, Universidad de Chile, are gratefully acknowledged.

References

Cifuentes, L., Glasner, R., Casas, J.M., 2004a. Aspects of the development of a copper electrowinning cell based on reactive electrodialysis. Chemical Engineering Science 59, 1087–1101.

Cifuentes, L., Mondaca, C., Casas, J.M., 2004b. The effectiveness of membrane systems for the separation of anolyte and catholyte in a lab-scale copper electrowinning cell based on reactive electrodialysis. Minerals Engineering 17, 803–809.

Cifuentes, L., Mella, M., 2006. On the physical quality of copper electrodeposits obtained on mesh cathodes. Canadian Metallurgical Quarterly 45, 9–15.

Cifuentes, L., Ortiz, R., Casas, J.M., 2005a. Electrowinning of copper using the Fe^{2+}/Fe^{3+} anodic reaction in a squirrel cage cell based on reactive electrodialysis. American Institute of Chemical Engineers' Journal 51, 2273–2284.

Cifuentes, L., Castro, J.M., Crisóstomo, G., Casas, J.M., Simpson, J., 2005b. Modelling a copper electrowinning cell based on reactive electrodialysis. Unpublished Results.

Scott, K., 1981. Moving bed electrolysis. US Patent no. 4 272 333.

Scott, K., 1988. A consideration of circulating bed electrodes for the recovery of metals from dilute solutions. Journal of Applied Electrochemistry 18, 504–510.

Stankovic, V.D., Stankovic, S., 1991. An investigation of the spouted bed electrode cell for the EW of metals from dilute solutions. Journal of Applied Electrochemistry 21, 124–129.